Nanoscale

PAPER

View Article Online
View Journal | View Issue

Cite this: *Nanoscale*, 2024, **16**, 7085

Silver-coated hollow fiber surface plasmon resonance sensor for glucose detection with enhanced limit of detection

Yangyang Xu, [a] Xian Zhang,[a] Xiao-Song Zhu *[a,b] and Yi-Wei Shi[a,b]

A fiber-optic surface plasmon resonance (SPR) biosensor based on a silver-coated hollow fiber (HF) structure for glucose detection is presented. The sensor surface was immobilized with 4-mercaptophenylboronic acid (PMBA) acting as a glucose recognition monolayer. Then, gold nanoparticles (AuNPs) modified with 2-aminoethanethiol (2-AET) and PMBA were introduced onto the sensor surface after glucose was captured to enhance the wavelength shift of the SPR phenomenon excited by the light transmitted in the wall of the HF sensor. Instead of the conventional one-step sensitization pretreatment commonly used in the deposition process of silver films for fiber-optic SPR sensors, a sensitization–activation two-step activation method was adopted in the fabrication of the proposed sensor. Experiments for glucose detection were performed on the fabricated sensors in the concentration range of 1 nM–1 mM. Results showed that the sensor fabricated by the two-step activation method has a much larger shift of resonance wavelength than the sensor fabricated using the one-step sensitization method. The resonance wavelength shift was found to be linear to the logarithm of the concentration in the range of 1 nM–1 mM. The sensor achieved a limit of detection (LOD) of as low as 1 nM, which is at least an order of magnitude lower than that of other fiber-optic sensors for glucose detection reported previously. The presented HF glucose sensor has the potential for biosensing applications and provides a large reference value in the study of optical fiber SPR sensors for biosensing.

Received 29th January 2024,
Accepted 4th March 2024

DOI: 10.1039/d4nr00421c

rsc.li/nanoscale

Introduction

Glucose is an essential substance and the most widely distributed monosaccharide in nature. It plays a pivotal role in the human body.[1–4] The increasing level of blood glucose content can result in many serious diseases, including hyperglycemia, diabetes, and cardiovascular disease.[5,6] As a result, the measurement of glucose concentration has received enormous attention in disease monitoring and medical research.[7–9] To date, various techniques have been reported for glucose detection, such as colorimetry[10,11] electrochemistry,[12,13] fluorometry,[14,15] and chemiluminescence assays.[16,17] Nevertheless, these methods often require complex operations and small detection ranges, which limit their scope of application. A surface plasmon resonance (SPR) sensor is based on sensing technology and has been extensively studied in the chemical and biological areas because of its superior optical properties and stable performance.[18–21] Compared with conventional prism-based SPR sensors, fiber-based optical sensors have the advantages of low-cost fabrication, anti-electromagnetic interference, small size, full biocompatibility, and remote online monitoring and have been widely used for the detection of glucose[22,23] and other trace molecules.[18,24] With the development of micro-structured optical fiber (MOF) technology, hollow fiber (HF) SPR sensors have received increasing attention because of their special structure.[25] Their hollow core can be used as a sample cavity to load a sample to be tested and avoid the problem of processing the cladding of fibers. Due to its relatively simple structure and excellent transmission performance, HF SPR sensors have become an analysis platform for both chemical and biological sensing areas.

Several methods have been reported for depositing a thin metal layer on MOF sensors.[26–29] Among these methods, electroless plating has exhibited potential over other methods in depositing a silver (Ag) film on an HF.[25,30] The surface of the HF substrate has no catalytic activity, and therefore, the surface catalysis process is an important pretreatment step.[31,32] Previous investigations indicate that activation is the necessary condition to determine the catalytic activity of the substrate and increase the reduction rate of plating metal ions.[33–35] The activation process of the substrate often uses a palladium chemical solution with high reactivity.[36,37] Previously reported HF SPR sensors are mostly based on the

[a]*School of Information Science and Technology, Fudan University, 220 Handan Rd, Shanghai 20433, China. E-mail: zhuxiaosong@fudan.edu.cn*
[b]*Key Laboratory for Information Science of Electromagnetic Waves (MoE), Fudan University, 220 Handan Rd, Shanghai 20433, China*

silver film deposited on the hollow fiber surface, which is fabricated using the one-step sensitization method.[25] Although the one-step activation pretreatment technology tends to be more mature, the poor durability and weak biocompatibility limit the chemical and biological sensing application of the HF sensor. Therefore, further pretreatment processes are usually required. Recently, the sensitization–activation two-step process has been applied as an optimal treatment method for electroless plating. This is because it offers the advantages of biochemical stability, biological compatibility and easy to form uniform coatings on the surface. Furthermore, the sensitization–activation two-step activation method can afford greater convenience and controllability, which is conducive to the preparation and practical application of the silver-coated HF sensor.

Boronic acid as the biological recognition element has been used in materials science applications as it can recognize the cis-diol configuration by forming a reversible complex.[5,38–40] In the detection of glucose concentration, 4-mercaptophenylboronic acid (PMBA) as a functionalization recognition molecule was introduced to the sensing region. In general, the detection of glucose, a small molecule, is through the covalent bonds between PMBA and glucose molecules in a sensing system of the optical fiber biosensor.[41] Moreover, consisting of Au nanoparticles (AuNPs) modified with the mixture of 2-aminoethanethiol (2-AET) and PMBA as the SPR signal amplified tags have been demonstrated for the detection of glucose.[22,41] Because the PH of the experimental condition needs a neutral environment in actual biological detection, we introduced 2-AET molecules in the process of functional nanoparticles. 2-AET was used to stabilize the SP^3 tetrahedral hybrid boron moiety of PMBA,[22,41,42] which is mainly because of the interaction of the amino groups ($–NH_2$) of the 2-AET molecule and boric acid.[42]

In this study, we report a fiber-optical SPR biosensor based on the silver-coated hollow fiber (HF) structure for glucose detection. The HF glucose sensor (HFGS) was fabricated with a self-assembled PMBA monolayer on silver film surfaces to capture glucose and then introduced 2-AET and PMBA-modified AuNPs to generate a typical sandwiched structure, leading to an enhancement in the wavelength shift of the SPR phenomenon excited by the light transmitted in the wall of the HF sensor. The sensitization–activation two-step activation deposition process was developed for coating a thin silver film on the inner surface of HF. In the experiments, the high sensitivity for glucose detection was achieved, and the concentration of glucose was detected by analyzing the change in the SPR wavelength. The experimental results showed that the resonance wavelength shift was found to be linear to the logarithm of concentration over the range of 1 nM–1 mM and the SPR shift of the sensor was largely enhanced. The proposed sensor achieved a low limit of detection (LOD) of 1 nM, which is at least an order of magnitude lower than that of other fiber-optic sensors for glucose detection reported previously. The objective was to provide a new solution in the optical fiber SPR-based glucose sensing way by offering a very stable and sensitive detection platform in the biosensing field.

Fabrication methods and experiments

Materials and apparatus

Gold acid chloride trihydrate ($HAuCl_4·3H_2O$), silver nitrate ($AgNO_3$, 99.8%), aqueous ammonia (~28%), palladium(II) chloride ($PdCl_2$), D-glucose and trisodium citrate dehydrate ($C_6H_5Na_3O_7$, 99%) were purchased from Sinopharm Chemical Reagent Co. Ltd (Shanghai, China). 2-AET (C_2H_7NS) was purchased from Energy Chemicals (Shanghai, China). D-Fructose, D-galactose, tin(II) chloride anhydrous ($SnCl_2$) and PMBA ($C_6H_7BO_2S$) were purchased from Aladdin Chemistry Co. Ltd (Shanghai, China). All chemicals and reagents used in the experiments were of analytical reagent grade and used without any further purification.

The UV-vis absorption spectra was measured using a UV-vis spectrometer (UV-3600, SHIMADZU). The structures and morphologies of the sensor and nanoparticles were characterized using a scanning electron microscope (SEM, Zeiss Gemini 300), and high-magnification transmission electron microscopy (TEM, JEM-F200). Raman spectra were measured using a portable Raman instrument (iHR-550, Horiba Jobin Yvon). Using the energy-dispersive X-ray (EDX) spectrometer present on the TEM instrument, the elemental distributions in the materials were mapped.

Fabrication of a silver film ($Ag/SnCl_2–PdCl_2$) coated on HF

A silver-coated HF was fabricated by coating a thin silver layer on the inner surface of the fused silica capillary by utilizing the electroless plating method. The schematic diagram of the deposition method of the silver layer is shown in Fig. 1. To acquire the smooth and uniform thin silver film, many factors in the deposition process need to be strictly controlled, such as the deposition time, solution flow rate, temperature, and pretreatment. There are two main steps in the deposition process: the pretreatment step and the silver deposition step.

Before the silver-plating process, the sensitization–activation two-step activation pretreatment was applied to the fused silica capillary. The diagram of the pretreatment process is shown in Fig. 1(a). Firstly, the fused silica capillary was washed successively with acetone, ethanol and deionized water. Subsequently, the pretreatment of the capillary consists

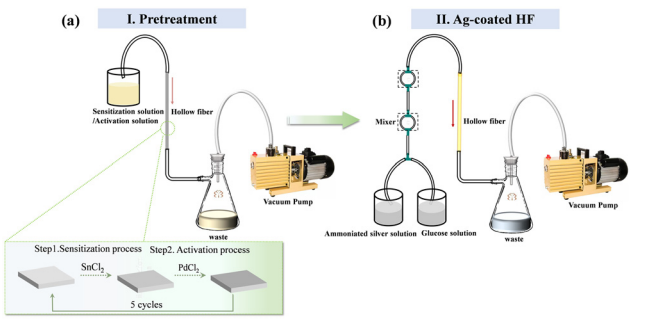

Fig. 1 Schematic diagram of the chemical liquid phase deposition method. (a) Pretreatment. (b) Silver deposition step.

of five cycles of a sensitizing process and an activation process. We used $SnCl_2$ as a sensitizing solution and $PdCl_2$ as an activation solution to sensitize and activate the inner surface of the silica tube alternately. The silica tube was washed thoroughly with the deionized water after each sensitizing and activation process. After the pretreatment step, the silver film was deposited on the inner surface of the sensitized-activated silica tube by the chemical liquid phase deposition method, as shown in Fig. 1(b). The silver mirror reaction was an optimum selection as a fast chemical liquid phase deposition method for coating silver film on the tube's inner surface. In our experiment, 5% ammoniacal silver solution in an alkaline solution and 5% glucose solution were used as the plating and reducing solutions, respectively. The solutions were mixed and forced to flow through the capillary by the vacuum pump at the flow rate of 25 ml min^{-1}. The reduced silver particles were adsorbed on the inner surface of the hollow fiber and gradually formed the silver film. Finally, the Ag-coated hollow fiber was carefully washed with distilled water and then blow-dried with nitrogen gas. For the prepared Ag-coated HF, the deposition time was 40 seconds and the reaction temperature was 19 °C.

AuNPs preparation and modification with 2-AET and PMBA

AuNPs used in the experiments were prepared by the reduction of chloroauric acid using sodium citrate.[43] 1 mL of 1% $HAuCl_4$ and 100 mL deionized water were mixed and heated to boiling under vigorous stirring, 4 mL of 1% aqueous trisodium citrate solution was then rapidly added, and the solution was kept boiling for 15 minutes and the color became deep wine. Finally, the mixture solution was cooled to room temperature with continuous stirring. The synthesis methods of 2-AET and PMBA-modified AuNPs have been reported previously.[22,41] The AuNPs/2AET–PMBA solution was obtained by mixing 15 μL of the mixture of 2-AET (1 mM) and PMBA (0.5 mM) in ethanol and adding to 10 mL of AuNPs with stirring for 15 minutes and then the functionalized AuNPs/2AET–PMBA was stored at 4 °C for 12 hours, as shown in Fig. 2(a).

Functional modification of the sensor

To fabricate the HFGS, four steps are required to functionalize the HF, as shown in Fig. 2(b). The Ag-coated HF was filled with anhydrous ethanol containing PMBA (10 mM) overnight to form the self-assembled monolayer (SAM) on the silver film of the sensing region in the sensor. Then the sensing region was rinsed thoroughly with deionized water (DIW) and dried. The PMBA-modified HFGS was filled with the aqueous glucose solutions of different concentrations for 20 minutes and then washed thoroughly with deionized water to remove unbound glucose. After that, the glucose-bound HFGS was filled with the AuNPs solution for 30 minutes. Then, the HFGS was rinsed with DIW. In the experiment, a 4 cm-long piece of fiber was cut off from the fabricated silver-coated HF to be used as the sensor is also shown in Fig. 2(b). In addition, the temperature was kept at 25 °C during the whole fabrication process.

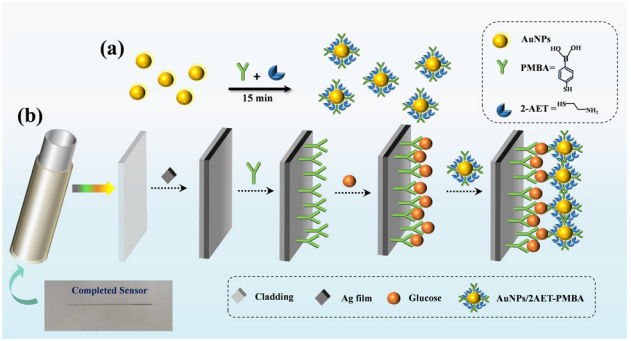

Fig. 2 Schematic illustration of the proposed sensor for glucose detection. (a) Preparation of the signal amplification tags (AuNPs/2AET–PMBA). (b) Self-assembly of PMBA on sensing surface and glucose sandwiched assay. Inset: image of the proposed sensor.

Experimental setup

The experimental system for glucose detection is illustrated in Fig. 3. The light beam emitted from a halogen lamp source is launched into the tubing wall of the HFGS *via* the multimode fiber bundles (MMFB). As shown in the inset of Fig. 3, the custom-made MMFB consists of six multimode fibers (MMFs) with a core/cladding diameter of 105/125 μm. The six MMFs were arranged in a ring to properly couple the input light into the tubing wall of the HFGS. The light propagated forward in the tubing wall of the HFGS and created the SPR phenomenon. The liquid with different samples was injected into the air holes of the HF sensor by the peristaltic pump from the end that was not spliced with the MMF. Owing to the hollow core and simple structure, the injection and exchange of the liquid could be completed within several seconds. The output light from the sensor was collected *via* the 600/660 μm MMF and detected by the spectrometer (PG2000-pro, Ideaoptics). Then, the SPR spectra of the light transmitted in the HFGS were obtained.

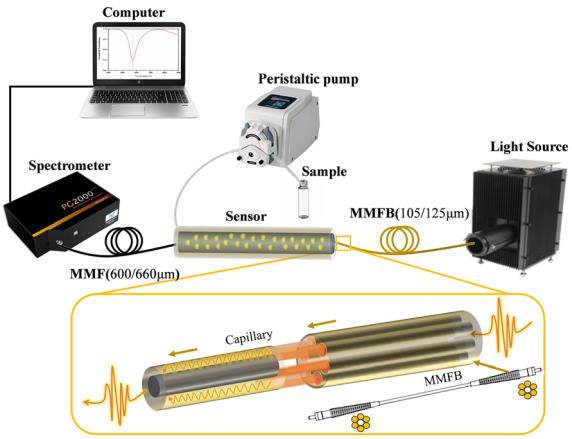

Fig. 3 Schematic diagram of the experimental setup.

Results and discussion

Characterization of gold nanoparticles modified with 2-AET and PMBA

As shown in the UV-vis spectra of Fig. 4(a), the absorbance peak of the AuNPs before and after the 2-AET and PMBA modification were both recorded at 519 nm. This result indicates that this functionalized modification method has no significant impact on the stability of the particles. The Raman spectroscopy data of the as-prepared AuNPs/2AET–PMBA are given in Fig. 4(b). The characteristic peaks of PMBA at 1570, 1070, 1019, and 996 cm^{-1} can be observed clearly, indicating the successful modification of AuNPs by the PMBA molecules. Moreover, the observed Raman bands at 415, 688, and 1472 cm^{-1} were attributable to the characteristic vibrational band modes of 2-AET. These vibrational bands coincide well with the previous reports.[22,40,41] According to Fig. 4(c), the TEM image demonstrated that the synthesized AuNPs/2AET–PMBA were spherical with a diameter of about 17 nm, which was quite homogeneous. The corresponding EDS-based elemental mapping images of AuNPs/2AET–PMBA (Fig. 4(d)) display the homogeneously distributed Au, S, B and N elements within the composite. These results further confirmed that the gold nanoparticles functionalized with PMBA and 2-AET were successfully prepared.

Characterization of the HFGS

Fig. 5 shows the morphologies of the cross-section and inner surface of the modified HFGS. As shown in Fig. 5(a), the HFGS shows the average inner and outer diameters of about 450 and 670 μm, respectively. The SEM photo of the cross-section of the silver film on the inner surface of HF is shown in Fig. 5(b). The thin silver film deposited on the surface can be seen clearly in the photo and the thickness was roughly measured as approximately 58.10 nm. Fig. 5(c) and (d) show that the sensing region before and after exposure to AuNPs/2AET–PMBA, the characterization results clearly reveal that AuNPs/2AET–PMBA are evenly distributed on the sensor surface.

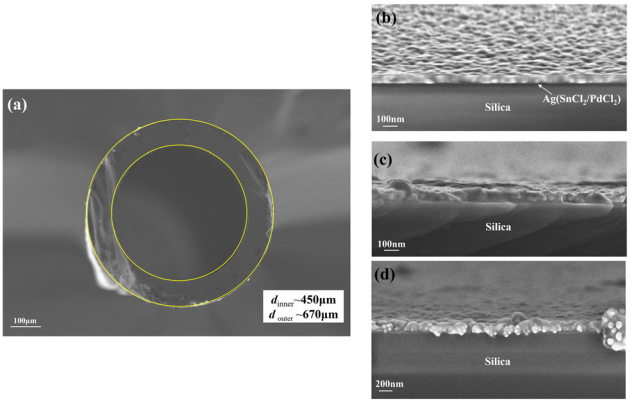

Fig. 5 (a) SEM image of the cross-section of the HFGS. (b) SEM images of the inner surfaces of the silver layer. (c) The sensing region without AuNPs/2AET–PMBA modification. (d) The sensing region with AuNPs/2AET–PMBA modification.

Glucose sensing

To verify the feasibility of the HFGS for glucose detection, two Ag-coated HF SPR sensors were fabricated with different pretreatment methods to compare the response in glucose sensing, including $SnCl_2$–$PdCl_2$ by two-step activation (Ag($SnCl_2$–$PdCl_2$)) and $SnCl_2$ *via* one-step activation (Ag($SnCl_2$)). The analyte filled in the HFGS was 1 mM aqueous glucose solution. Fig. 6 shows the transmission spectra of the two HFGS. As shown in the spectra, the resonance wavelength shifted toward the long wavelength direction when the PMBA modified the sensor surface, indicating that PMBA was adsorbed on the surface of the Ag-coated optical fiber through the formation of an Ag–S bond. A slight shift in the resonance wavelength shift ($\Delta\lambda$) was obtained when the PMBA-modified SPR sensing surface interacted with glucose. However, when AuNPs/2AET–PMBA was injected, the SPR dip red-shifted significantly. These results indicated that the Au NPs/2AET–PMBA were captured onto the Ag film by glucose molecules as

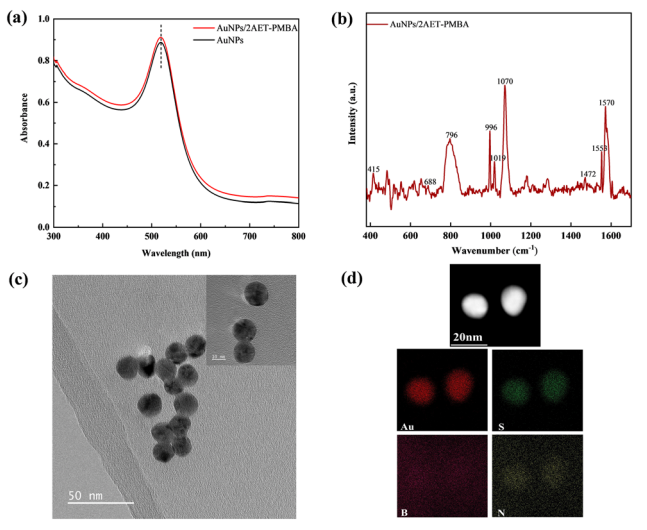

Fig. 4 Analysis of AuNPs/2AET–PMBA. (a) UV-vis absorption spectra of Au NPs and AuNPs/2AET–PMBA. (b) Raman spectrum of AuNPs/2AET–PMBA. (c) TEM image of AuNPs/2AET–PMBA. (d) EDX analysis of AuNPs/2AET–PMBA.

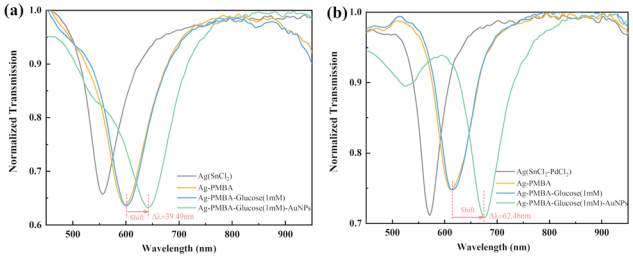

Fig. 6 The variation of SPR spectra for glucose detection for the sensors fabricated by two different pretreatment methods (a) Ag($SnCl_2$). (b) Ag($SnCl_2$–$PdCl_2$).

SPR signal amplification tags. As shown in Fig. 6(a) and (b), the resonant wavelength shift for the $Ag(SnCl_2)$ activation approach was only 39.49 nm, which was much less than the 62.46 nm shift for the sample $Ag(SnCl_2–PdCl_2)$ prepared by the two-step activation approach. Such results indicate that the shift of the SPR wavelength of the HFGS is largely enhanced by adopting the $SnCl_2–PdCl_2$ two-step activation method instead of the $SnCl_2$ one-step activation method, which is conventionally used in the fabrication of HF SPR sensors. The larger shift of the SPR wavelength means a larger sensitivity for the wavelength interrogation SPR sensor. Thus, the performance of the HFGS is enhanced by the $SnCl_2–PdCl_2$ two-step activation approach in the fabrication procedure. Moreover, the two-step activation method improves the adhesion between the glass surface, and the silver particles were reduced in the silver mirror reaction, which makes the coated silver film more durable.[44] The HFGSs used in the follow-up experiments were fabricated by the two-step activation method.

Real-time detection of glucose

Experiments of glucose detection were performed using the fabricated HFGS to evaluate its performance. The transmission spectra were measured during the whole glucose detection process, and the dynamic change of the resonance wavelengths is shown in Fig. 7(a). Here, the concentration of glucose solution is 1 mM. Before injection of the glucose solution, DIW flowed through the sensor (stage I). After baseline stability was reached, the wavelength variation was recorded continuously. In stage II, there was only a slight shift in the SPR wavelength after injecting the glucose solution due to the slight changes in the surface refractive index during the PMBA and glucose molecular binding process. The PMBA has the ability to capture the glucose molecule because the boronic acid group interacts with one set of syn-periplanar diol groups of glucose. After that, the nonspecific binding of glucose molecules was removed through the injection of water (stage III). Then, AuNPs/2AET–PMBA solution was injected into the sensing system (stage IV); it was found that the SPR wavelength experienced a significant shift in the direction of longer wavelength. It can be attributed to the fact that the boronic acid group of Au NPs/2AET–PMBA binds with another set of syn-periplanar diol groups of glucose. This is mainly due to the fact that AuNPs enhance the signal through their high mass, and more importantly, a strong electric field was generated between the Ag film and AuNPs, forming a particular sandwiched structure and enhancing the SPR signal greatly. The shift of the SPR wavelength continues to increase over time and nearly reaches saturation after approximately 1200 seconds. Finally, the sensor was washed with DIW to remove the unbound AuNPs (stage V).

Glucose solutions with different concentrations were introduced into the sensor in order to verify the sensitivity and the linearity of the proposed sensor. Fig. 7(b) presents the variation of the SPR wavelength for glucose detection without AuNPs. When the low-concentration glucose solutions (1 nM–0.1 mM) were injected into the sensing system, the resonance wavelength did not show an obvious shift. Because the glucose molecule is too small, it has inadequate mass to produce a measurable change in the refractive index on the surface of the SPR sensor at low concentration, resulting in the difficulty of direct glucose detection by SPR without any enhancement. Thus, the obtained AuNPs can be used as a signal amplification tag to elicit SPR signal amplification. Similar experiments were also performed with DIW (labeled as 0 nM) and seven glucose solutions of different concentrations ranging from 1 nM to 1 mM. The responses in the SPR wavelength shift in stage IV are shown in Fig. 7(c). For all concentrations of glucose, the shifts have the same trend of variation, increasing continuously over time and reaching saturation subsequently. The maximum shift increases with the increasing concentration of glucose.

Fig. 7(d) shows the shift of SPR wavelength as a function of glucose concentrations in the range of 1 nM to 1 mM. The wavelength shift with the concentration conforms to the well-known Langmuir isotherm model with an excellent correlation coefficient of R^2 = 0.98127. Moreover, as shown in the inset, the wave-

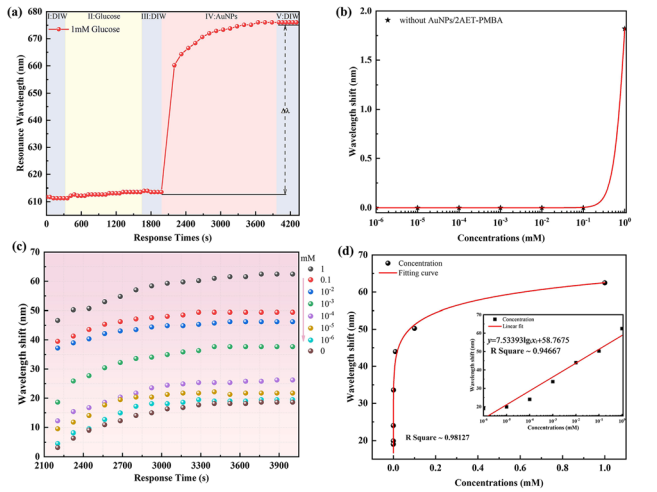

Fig. 7 Experimental performance of the HFGS in glucose detection. (a) Real-time variation of SPR wavelength in 1 mM glucose detection. I: DIW. II: glucose. III: DIW. IV: AuNPs/2AET–PMBA. V: DIW. (b) The shift in the resonance wavelength for glucose detection without AuNPs/2AET–PMBA. (c) The wavelength shift in the presence of AuNPs/2AET–PMBA for different concentrations of glucose (from 1 nM to 1 mM). (d) Calibration curves for glucose detection results. Inset: linear calibration curve between the SPR wavelength shift and the logarithm of glucose concentration.

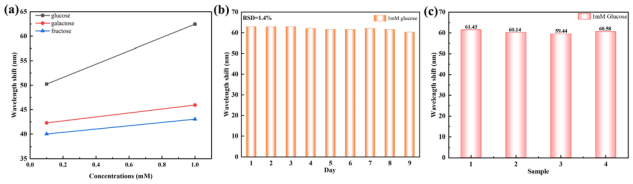

Fig. 8 (a) The shift of SPR wavelength with different saccharides. (b) The stability test for different days (1–9 days). (c) The results of four HFGSs for the detection of 1 mM glucose.

Table 1 Comparison between HFGS and other fiber-optic SPR sensors for glucose detection

Detection method	Linear range	LOD	Ref.
Fiber-optic/AuNPs-PMBA	80 nM–30 mM	80 nM	22
Fiber-optic/PBMA	0–1.7 mM	0.00078 mM	42
Fiber-optic/CQDs-COD/CA	10 nM–200 μM	25.79 nM	45
Fiber-optic/PMBA	10 mM–50 mM	0.2 mM	46
Dual-channel fiber/GOx	0–1.5 mM	16.24 μM	47
Dual-parameter fiber/PMBA	0–4 mM	1.136 μM	48
Prism coupler/Au layer UiO-66/$Au_{0.5}$ layer	0.01–10 mM	0.0693 mM	49
Prism coupler/Au/Zr-BDC film	0.1–20 mM	0.482 mM	50
Hollow fiber/AuNPs-PMBA	1 nM–1 mM	1 nM	This work

length shift presents a linear relationship to the logarithm value of glucose concentration in the range of 1 nM to 1 mM. The sensitivity of 7.534 nm per lg (mM) is obtained by calculating the slope of the linear fitting to the experimental results. Usually, the LOD of such a kind of sensor is defined as the concentration corresponding to three times the standard deviation (SD) of the system noise. The SD of the measured resonance wavelength was obtained as 0.04 nm by measuring the spectra 36 times. The difference in the resonance wavelength between 1 nM glucose and DIW is 0.46 nm, which is still larger than the triple SD, *i.e.* 0.12 nm. Therefore, the presented HFGS could achieve LOD as low as 1 nm at least for glucose detection.

Selectivity, stability and repeatability of the HFGS

To test the selectivity of the sensor, we selected some saccharides with the diol configurations that exist in actual detection samples and have relatively similar properties for experiments. In this experiment, glucose, fructose and galactose were selected as the samples for testing. The comparative analysis of all samples was performed with two different concentrations (1 mM, 0.1 mM). The results of the selectivity experiment are shown in Fig. 8(a). It can clearly be seen that the sensor shows a maximum wavelength shift in glucose detection over other saccharides. Owing to the fact that glucose has two sets of cis-diol configurations, the combination of an Ag-coated HF sensor with PMBA and AuNPs shows a much stronger affinity to glucose molecules. Besides, these results indicated that the HFGS has good selectivity. The stability of the sensor for glucose (1 mM) was examined at room temperature for 9 days. The measured spectra for DIW are shown in Fig. 8(b). The wavelength shift has no obvious change with an average relative standard deviation (RSD) of 1.4%, demonstrating good stability of the sensor. The proposed sensor displays stability for at least one week.

Furthermore, we also investigated the repeatability of the HFGS. Experiments for the detection of 1 mM glucose were performed using four HFGSs fabricated with the same procedure and parameters. The SPR wavelength shifts of the four HFGSs are shown in Fig. 8(c). There is a good consistency of the four sensors with an average resonance wavelength shift at 60.40 nm, showing an RSD of less than 2%. Hence, the presented HFGS possesses good repeatability. Table 1 shows the comparison between the proposed sensor and other SPR sensors for glucose detection. It can be seen that HFGS has a much lower LOD, which is at least an order of magnitude lower than that of other fiber-optic sensors. Additionally, the proposed sensor may not be very suitable for the common glucose level monitoring of diabetes patients since the LOD is considerably lower than the physiological level of glucose in the blood (3–8 mM). However, it can be used for monitoring and high-precision glucose sensing in similar fields such as pharmaceutical analysis and the food industry.

Conclusions

In summary, we proposed and demonstrated an SPR biosensor based on the silver-coated HF structure for sensitive and stable low-concentration glucose detection. The HF glucose sensor was fabricated through the use of a self-assembled PMBA monolayer on the silver-coated HF and the signal amplification tags of AuNPs modified with 2-AET and PMBA, forming a typical sandwiched structure and enhancing the wavelength shift of the SPR phenomenon excited by the light transmitted in the wall of the HF sensor. Herein, the silver film was plated on the HF by using the sensitization–activation two-step activation pretreatment method instead of the conventional one-step sensitization. The glucose solution was filled in the hollow core of the HF and its concentration could be detected by measuring the transmission spectra of the HF sensor. The experimental results show that the sensor fabricated by the two-step activation method has a much larger shift of resonance wavelength than the sensor fabricated by the one-step sensitization method. The HF glucose sensor has an LOD of 1 nM with a wide linear range from 1 nM to 1 mM, which is at least an order of magnitude lower than that of most reported fiber-optic sensors. The presented HF glucose sensor has potential in biosensing applications and provides a large reference value to the study of optical fiber SPR sensors for biosensing. Moreover, the presented pretreatment method could contribute to the research of optical fiber SPR sensors.

Author contributions

Yangyang Xu: conceptualization, investigation, sample preparation, writing – original draft. Xian Zhang: formal analysis,

investigation. Xiao-Song Zhu: conceptualization, writing – review and editing, funding acquisition, supervision. Yi-Wei Shi: supervision. All authors have read and agreed to the published version of the manuscript.

Conflicts of interest

There are no conflicts to declare.

Acknowledgements

This work was supported by the National Natural Science Foundation of China (grant no. 61975034).

References

1 Y. Oh, J. S. Y. Lai, J. H. Mills, H. Erdjument-Bromage, B. Giammarinaro and K. Saadipour, *Nature*, 2019, **574**, 559–564.
2 X. C. Sun, *Anal. Chim. Acta*, 2022, **1206**, 339226.
3 H. J. Jeon, S. Kim, S. Park, I. K. Jeong, J. Kang and Y. R. Kim, *Nano Lett.*, 2021, **21**, 8933–8940.
4 C. X. Zhang, C. J. Wei, D. J. Chen, Z. K. Xu and X. J. Huang, *Sens. Actuators, B*, 2023, **385**, 133630.
5 X. G. Li, F. Zhang, Y. Gao, Q. M. Zhou, Y. Zhao, Y. Li, J. Z. Huo and X. J. Zhao, *Biosens. Bioelectron.*, 2016, **86**, 270–276.
6 P. Q. Gong, X. G. Li, X. Zhou, Y. A. Zhang, N. Chen, S. K. Wang, S. Q. Zhang and Y. Zhao, *Opt. Laser Technol.*, 2021, **139**, 106981.
7 W. L. Brooks and B. S. Sumerlin, *Chem. Rev.*, 2015, **116**, 1375–1397.
8 M. Adeel, K. Asif, M. M. Rahman, S. Daniele, V. Canzonieri and F. Rizzolio, *Adv. Funct. Mater.*, 2021, **31**, 2106023.
9 A. H. Almawgani, S. A. Taya, M. G. Daher, I. Colak, F. Wu and S. K. Patel, *Phys. Scr.*, 2022, **97**, 065501.
10 H. J. Jeon, H. S. Kim, E. Chung and D. Y. Lee, *Theranostics*, 2022, **12**, 6308–6338.
11 J. Y. Xiao, Y. Liu, L. Su, D. Zhao, L. Zhao and X. J. Zhang, *Anal. Chem.*, 2019, **91**, 14803–14807.
12 C. H. He, M. Asif, Q. Q. Liu, F. Xiao, H. F. Liu and B. Y. Xia, *Adv. Mater. Technol.*, 2022, **8**, 2200272.
13 H. Teymourian, A. Barfidokht and J. Wang, *Chem. Soc. Rev.*, 2020, **49**, 7671–7709.
14 L. P. Feng, J. N. Yang, S. Zhang, L. X. Zhang, X. Chen, P. Li, Y. Gao, S. J. Xie, Y. Zhang and H. Wang, *Analyst*, 2020, **145**, 5273–5279.
15 T. Han, S. M. Zhu, S. C. Wang, B. J. Wang, X. J. Zhang and G. F. Wang, *Mikrochim. Acta*, 2019, **186**, 1–9.
16 D. J. Li, S. S. Zhang, X. Feng, H. J. Yang, F. Nie and W. Y. Zhang, *Sens. Actuators, B*, 2019, **296**, 126631.
17 Y. Duan, Y. J. Huang, S. Y. Chen, W. Y. Zuo and B. F. Shi, *ACS Omega*, 2019, **4**, 9911–9917.
18 Y. Zhao, R. J. Tong, F. Xia and Y. Peng, *Biosens. Bioelectron.*, 2019, **142**, 111505.
19 J. Ashley, M. Piekarska, C. Segers, L. Trinh, T. Rodgers, R. Willey and I. E. Tothill, *Biosens. Bioelectron.*, 2017, **88**, 109–113.
20 C. X. Teng, R. Min, J. Zheng, S. J. Deng, M. S. Li, L. Hou and L. B. Yuan, *Sensors*, 2021, **22**, 81.
21 N. K. Singh, B. Jain and S. Annapoorni, *Sens. Actuators, B*, 2011, **156**, 383–387.
22 H. Z. Yuan, W. Ji, S. W. Chu, S. Y. Qian, F. Wang, J. F. Masson and W. Peng, *Biosens. Bioelectron.*, 2018, **117**, 637–643.
23 H. X. Yu, Y. Chong, P. Z. Zhang, J. M. Ma and D. C. Li, *Talanta*, 2020, **219**, 121324.
24 L. X. Li, Y. Z. Liang, J. Y. Guang, W. L. Cui, X. P. Zhang, J. F. Masson and W. Peng, *Opt. Express*, 2017, **25**, 26950–26957.
25 B. H. Liu, Y. X. Jiang, X. S. Zhu, X. L. Tang and Y. W. Shi, *Opt. Express*, 2013, **21**, 32349–32357.
26 Y. Z. Liang, W. L. Cui, L. X. Li, Z. Y. Yu, W. Peng and T. Xu, *Adv. Opt. Mater.*, 2019, **7**, 1801269.
27 Z. H. Liu, W. Liu, B. Lai, Y. Zhang, Y. X. Zhang, X. H. Yang, J. Z. Zhang and L. B. Yuan, *Opt. Express*, 2021, **29**, 18305–18314.
28 A. A. Rifat, G. A. Mahdiraji, D. M. Chow, Y. G. Shee, R. Ahmed and F. R. M. Adikan, *Sensors*, 2015, **15**, 11499–11510.
29 C. Liu, J. W. Wang, F. M. Wang, W. Q. Su, L. Yang, J. W. Lv, G. L. Fu, X. L. Li, Q. Liu, T. Sun and P. K. Chu, *Opt. Commun.*, 2020, **464**, 125496.
30 X. Zhang, Y. Y. Xu, X. S. Zhu and Y. W. Shi, *Opt. Express*, 2023, **31**, 26398–26409.
31 H. W. Pang, R. C. Bai, Q. S. Shao, Y. F. Gao, A. J. Li and Z. Y. Tang, *Appl. Surf. Sci.*, 2015, **359**, 280–287.
32 Y. Kobayashi, V. Salgueiriño-Maceira and L. M. Liz-Marzán, *Chem. Mater.*, 2001, **13**, 1630–1633.
33 J. K. Pancrecious, S. B. Ulaeto, R. Ramya, T. P. D. Rajan and B. C. Pai, *Int. Mater. Rev.*, 2018, **63**, 488–512.
34 C. C. Liu, X. L. Li, X. Q. Li, T. Z. Xu, C. Y. Song and K. J. Ogino, *Materials*, 2018, **11**, 2033.
35 N. J. Li, N. W. Li, M. M. Li and D. Yi, *Appl. Mech. Mater.*, 2013, **423**, 837–841.
36 L. Wei, J. Yu, X. J. Hu, R. X. Wang and Y. Huang, *Chin. J. Chem. Eng.*, 2016, **24**, 1154–1160.
37 S. Huang, J. Wang, Y. Li, J. Tang and X. Zhang, *Appl. Surf. Sci.*, 2020, **516**, 146134.
38 S. Y. Qian, Y. Zhang, H. Z. Yuan, W. Ji, Y. Liu, J. Z. Zhao, M. Han and W. Peng, *Sens. Actuators, B*, 2018, **260**, 976–982.
39 Z. C. Bian, A. Q. Liu, Y. Li, G. Q. Fang, Q. Q. Yao, G. M. Zhang and Z. Y. Wu, *Analyst*, 2019, **145**, 719–744.
40 X. S. Bi, X. Z. Du, J. J. Jiang and X. Huang, *Anal. Chem.*, 2015, **87**, 2016–2021.
41 F. Wang, M. D. Lu, H. Z. Yuan, Y. Zhang, W. Ji, C. S. Sun and W. Peng, *J. Lightwave Technol.*, 2021, **39**, 3882–3889.

42 W. L. Zheng, Y. N. Zhang, L. K. Li, X. G. Li and Y. Zhao, *Biosens. Bioelectron.*, 2022, **198**, 113798.
43 K. C. Grabar, R. G. Freeman, M. B. Hommer and M. J. Natan, *Anal. Chem.*, 1995, **67**, 735–743.
44 W. Li, Y. Chen, S. Wu, J. Zhang, H. Wang, D. Zeng and C. Xie, *Appl. Surf. Sci.*, 2018, **436**, 117–124.
45 S. Yu, L. Y. Ding, H. T. Lin, W. Wu and J. Huang, *Biosens. Bioelectron.*, 2019, **146**, 111760.
46 S. Y. Qian, Y. Z. Liang, J. Ma, Y. Zhang, J. Z. Zhao and W. Peng, *Sens. Actuators, B*, 2015, **220**, 1217–1223.
47 S. N. Wu, Q. Tan, E. Forsberg, S. Q. Hu and S. L. He, *Opt. Express*, 2020, **28**, 21046–21061.
48 X. Wang, X. Sun, Y. Hu, L. Zeng and J. A. Duan, *Optik*, 2023, **284**, 170933.
49 G. Gumilar, J. Henzie, B. Yuliarto, A. Patah, N. Nugraha, M. Iqbal, A. A. Mohammed, M. S. A. Hossain, Y. Yamauchi and Y. V. Kaneti, *J. Mater. Chem. A*, 2022, **10**, 6662–6678.
50 G. Gumilar, S. Chowdhury, G. Shukri, A. Patah, N. Nugraha, J. Henzie, I. Anshori, Y. V. Kanetid and B. Yuliarto, *J. Mater. Chem. B*, 2023, **11**, 4428–4444.